

The “amplitude” parameter of Gamma-Ray Bursts and its implications for GRB classification

Hou-Jun Lü¹, Bing Zhang¹*, En-Wei Liang^{2,1}, Bin-Bin Zhang³ and Takanori Sakamoto⁴

¹*Department of Physics and Astronomy, University of Nevada, Las Vegas, NV 89154, USA*

²*Department of Physics and GXU-NAOC Center for Astrophysics and Space Sciences, Guangxi University, Nanning 530004, China*

³*Center for Space Plasma and Aeronomic Research (CSPAR), University of Alabama in Huntsville, Huntsville, AL 35899, USA*

⁴*Department of Physics and Mathematics, Aoyama Gakuin University, Sagami-hara-shi Kanagawa 252-5258, Japan*

21 February 2022

ABSTRACT

Traditionally gamma-ray bursts (GRBs) are classified in the T_{90} -hardness ratio two-dimensional plane into long/soft and short/hard GRBs. In this paper, we suggest to add the “amplitude” of GRB prompt emission as the third dimension as a complementary criterion to classify GRBs, especially those of short durations. We define three new parameters f , f_{eff} and $f_{\text{eff},z}$ as ratios between the measured/simulated peak flux of a GRB/pseudo-GRB and the flux background, and discuss the applications of these parameters to GRB classification. We systematically derive these parameters to find that most short GRBs are likely not “tip-of-iceberg” of long GRBs. However, one needs to be cautious if a short GRB has a relatively small f (e.g. $f < 1.5$), since the chance for an intrinsically long GRB to appear as a “disguised” short GRB is higher. Based on available data, we quantify the probability of a disguised short GRB below a certain f value is as $P(< f) \sim 0.78_{-0.4}^{+0.71} f^{-4.33 \pm 1.84}$. By progressively “moving” a long GRB to higher redshifts through simulations, we also find that most long GRBs would show up as rest-frame short GRBs above a certain redshift.

Key words: gamma-ray bursts: general — methods: statistical

1 INTRODUCTION

Traditionally, gamma-ray bursts (GRBs) are classified based on duration (T_{90}) and hardness ratio (HR) of their prompt gamma-ray emission. In the CGRO/BATSE era, GRBs were classified into two categories in the T_{90} -HR two-dimensional plane (Kouveliotou et al. 1993) with a rough separation in the duration dimension at $T_{90} \sim 2$ s. Long GRBs are typically soft while short GRBs are typically hard, so that the two classes cluster in two regions in the T_{90} -HR plane. Such a distribution is energy-dependent and instrument-dependent (e.g. Qin et al. 2013; Zhang et al. 2012). A third, intermediate class has been suggested by various authors based on the duration criterion alone (e.g. Mukherjee et al. 1998; Horvath 1998; Hakkila et al. 2000; Horvath et al. 2010).

Broad-band afterglow observations of long GRBs reveal that their host galaxies are typically irregular galaxies with intense star formation (Fruchter et al. 2006). Some long GRBs are firmly associated with Type Ib/c supernova (e.g. Hjorth et al. 2003; Stanek et al. 2003; Campana et al. 2006; Pian et al. 2006; Xu et al. 2013). This strongly suggests that

they are likely related to the deaths of massive stars, and the “collapsar” model has been widely accepted to be the standard paradigm for long GRBs (Woosley 1993; MacFadyen & Woosley 1999). Detections of afterglows and host galaxies of short GRBs in the Swift (Gehrels et al. 2004) era have advanced our understanding of their physical origin. Some short GRBs are found to be associated with nearby early-type galaxies with little star formation (Gehrels et al. 2005; Bloom et al. 2006; Barthelmy et al. 2005; Berger et al. 2005), or have a large offset from the host even if they are associated with star forming galaxies (e.g. Fox et al. 2005; Fong et al. 2010). Deep upper limits of their supernova signals are obtained (Kann et al. 2011, Berger 2014 and references therein). This points towards an origin that does not involve a massive star. The leading scenario is mergers of two neutron stars (Paczýnski 1986; Eichler et al. 1989) or mergers of a neutron star and a black hole (Paczýnski 1991b). There is no evidence that the intermediate third class forms a physically distinct population of GRBs.

Further observations revealed a more complicated picture, suggesting that duration is no longer a reliable indicator of the physical origin of a GRB. The detections of two nearby long-duration GRBs without association of a super-

* E-mail: lhj@physics.unlv.edu, zhang@physics.unlv.edu

nova, i.e. GRB 060614 ($T_{90} \sim 100$ s at $z = 0.125$) and GRB 060505 ($T_{90} = 4$ s at $z = 0.089$), cast doubts on that all long GRBs are of a massive star origin (Gehrels et al. 2006; Gal-Yam et al. 2006; Fynbo et al. 2006; Della Valle et al. 2006). On the other hand, some properties of GRB 060614 (e.g. short spectral lag, Gehrels et al. 2006) and the large offset from the star forming region in the host (Gal-Yam et al. 2006) are consistent with being a compact star origin. Zhang et al. (2007b) showed that if GRB 060614 were somewhat less energetic, it would appear as quite similar to GRB 050724, which is the “smoking gun” short GRB (with extended emission) that suggests a compact star origin (Barthelmy et al. 2005; Berger et al. 2005). Later, several high- z GRBs with the rest frame duration $T_{90}/(1+z)$ shorter than 2 s were discovered: GRB 080913 at $z = 6.7$ with $T_{90} = 8$ s (Greiner et al. 2009), GRB 090423 at $z = 8.2$ with $T_{90} = 10.3$ s (Tanvir et al. 2009; Salvaterra et al. 2009), and GRB 090429B at $z = 9.4$ with $T_{90} = 5.5$ s (Cucchiara et al. 2011), but various arguments suggest that they are of a massive star origin (Zhang et al. 2009). Later, more traditional short GRBs are found to be likely of a massive star origin. For example, GRB 090426, at $z = 2.609$, is found to have an observed BAT band duration $T_{90} = 1.2 \pm 0.3$ s and a rest frame duration $T_{90}/(1+z) \sim 0.33$ s, but its other properties are fully consistent with being of a massive star origin (Levesque et al. 2010; Xin et al. 2011; Thöne et al. 2011).

In view of these complications, Zhang (2006) and Zhang et al. (2007b) suggested to classify GRBs physically into Type II (massive star origin) and Type I (compact star origin). Zhang et al. (2009) studied the statistical properties of the Type II and Type I Gold Samples, and found that although the Type II Gold sample tracks the bulk of long GRBs well, the Type I Gold sample is not a good representative of the short GRBs. They suggested a set of multi-wavelength criteria to diagnose the physical origin of GRBs (see also Kann et al. 2011), and suspected that some, maybe most high-redshift high-luminosity short GRBs would be of a Type II origin. This conclusion was later also drawn by several groups independently based on very different arguments (Virgili et al. 2011; Cui et al. 2012; Bromberg et al. 2012).

Even though the multi-wavelength criteria can give more definite clues about the origin of a GRB, they are not available promptly after the trigger of the GRB. Some criteria that carry most weight (e.g. supernova signature, host galaxy information) need late, deep optical observations. It is still useful to apply the prompt gamma-ray data to dig out more information, which may be helpful to infer the physical origin of a GRB. For example, in Lü et al. (2010), we have proposed a new observational parameter ε defined by $E_{\gamma,iso}/E_{p,z}^{5/3}$, where $E_{\gamma,iso}$ is the burst isotropic gamma-ray energy and $E_{p,z}$ is the rest-frame spectral peak energy. This parameter has a cleaner bimodal distribution, and the two types of burst classified with the ε criterion match the physical classification scheme (Type I vs. Type II) better. This method still needs the redshift information.

In this paper, we propose to add a third dimension “amplitude” into consideration to classify GRBs using the prompt gamma-ray data (see a preliminary discussion in Zhang 2012). The motivation is to study the possibility that a real long GRB may be observed as a “short” one if the ma-

jority of emission episode is too faint to be detected above the background. We call this the “tip-of-iceberg” effect¹. To quantify this effect, in Sect. 2, we introduce a new “amplitude parameter” f , and study the distribution of *Swift* GRBs in the three-dimensional ($T_{90} - \text{HR} - f$) space. In Sect. 3, we introduce an effective amplitude parameter f_{eff} to discuss the range of amplitude if a long GRB is observed as “short” due to the tip-of-iceberg effect. We compare the range of f distribution of short GRBs and the f_{eff} distribution of long GRBs and suggest a confusion regime of f where an observed short GRB may be in fact long. In Sect. 4, we define a parameter $f_{\text{eff},z}$ by “moving” GRBs with known redshift to higher redshifts through simulations until they become “rest-frame short” GRBs. We take GRB 080319B as an example, and show that long GRBs can become rest-frame short GRBs at high enough redshifts, but with a moderately large f . We show that this is consistent with the three highest- z GRBs: 080913, 090423 and 090429B. We draw conclusions in Sect. 5 with some discussion.

2 THE AMPLITUDE PARAMETER F

In the previous T_{90} -HR two-dimensional diagram, the amplitude information of GRBs is missing. Some GRBs can be very bright, while some others can be faint and barely above the threshold. A bright burst can have more emission episodes emerging above the background, so for a same observed T_{90} , a fainter burst may be intrinsically longer than a brighter burst. So this third dimension, i.e. the “amplitude”, carries important information and should be introduced in GRB classification studies. Such a fluence truncation effect has been studied extensively in the past (e.g. Koshut et al. 1996; Bonnell et al. 1997; Hakkila et al. 2000; Schmidt 2001).

Here we quantify such an effect by defining an amplitude parameter

$$f \equiv \frac{F_p}{F_B}, \quad (1)$$

where F_p is the 1-second peak flux on the gamma-ray emission lightcurve, and F_B is the average background flux of the burst. Both fluxes are in units of count rate.

We systematically process the *Swift* Burst Alert Telescope (BAT) GRB data to extract lightcurves. We developed an IDL script to automatically download and maintain all the *Swift* BAT data. We use the standard HEASoft tools (version 6.12) to process the data. By running *bateconvert* from the HEASoft software release, we obtain the energy scale for the BAT events. The lightcurves are extracted by running *batbinevt* (Sakamoto et al. 2007). For each burst, we calculate the cumulative distribution of the source count using the arrival times of a fraction of 5% and 95% of the total counts to define T_{90} (see Fig 5). The time bin size is fixed to 64 ms for all the bursts. Background is extracted using two time intervals, one before and one after the burst. By fitting the background as a Poisson noise, one can obtain its

¹ In the early BATSE era, some authors had introduced the effective amplitude parameters such as V/V_{max} or $C_{\text{max}}/C_{\text{min}}$ to perform statistical analyses, but the purpose of their studies was to test for the uniformity of the GRB spatial distribution (e.g. Schmidt et al. 1988; Paczynski 1991a).

standard deviation. The error of f is derived from the error of F_B based on error propagation.

Our sample includes the GRBs detected by *Swift* BAT from December 2004 to December 2011. We only selected 437 GRBs with S/N ratio higher than 5, which include 395 long GRBs and 42 short GRBs. Among them, 182 have redshift measurements. For each GRB, we fit the background flux level F_B using the time intervals before and after the burst. This background is burst-dependent, but is around a value of 8000 cts/s. For a small fraction (6.8%) of the bursts, the background before and after the burst is uneven. This is because some bright hard X-ray sources could be entering or exiting the BAT field of view during the slew. For these cases, we fit the background before and after the burst with a straight line with a slope. F_B is defined by fitted background flux at the peak time². Figure 1 shows the histogram of F_B for all the GRBs in our sample.

The f values of the GRBs in our sample are presented at <http://grb.physics.unlv.edu/f/data.txt>. The T_{90} – HR – f 3-dimensional distribution diagram of *Swift* GRBs is shown in Fig.2. Long and short GRBs are denoted as black and white symbols. The projections in the T_{90} – HR, T_{90} – f and HR – f planes are denoted in red, green, and blue colors, respectively, with long and short GRBs denoted by the filled and open symbols, respectively. In Fig.3a, we show 1D distribution (T_{90} and f), and 2D (T_{90} – f) diagram with different symbols denoting different types of GRBs: gray for long GRBs, red for short GRBs, blue for short GRBs with extended emission (T_{90} calculated by excluding the extended emission), purple for the three “rest-frame short” ($T_{90}/(1+z) < 2$ s) high- z GRBs, black for other “rest-frame short” GRBs, and two special GRBs, 090426 and 060614, are marked separately.

The distributions of the f -parameter for both long and short GRBs are presented in Fig.4a. As expected, Most bursts are clustered around small f values, and only a small fraction of bursts have $f > 3$. The f distribution can be roughly fit as a power law function, i.e. $N(f) \propto f^{-a}$, with $a \sim 3.54$ for long GRBs and $a \sim 1.66$ for short GRBs. The mean value of f is $\bar{f} = 1.48$ for long GRBs and $\bar{f} = 1.82$ for short GRBs. The largest f values for both long and short GRBs are around 10. The relative paucity of small f for short GRBs may be understood as a selection effect (Sakamoto et al. 2008, 2011): Short GRBs are detected via “rate triggers”, which require a relatively large f value to meet the trigger criterion. On the other hand, long GRBs can be caught via “imaging triggers” near the threshold, so that they can be detected with lower f values close to unity.

Although the average value f of long GRBs is smaller than short GRBs, and the $N(f) \propto f^{-a}$ slope of the two populations are considerably different, one cannot significantly improve the duration classification scheme with the introduction of the f value. As shown below, when introducing the next parameter f_{eff} , one can gain useful information to

judge the true duration category of a GRB, especially for short GRBs.

3 EFFECTIVE AMPLITUDE F_{EFF} OF LONG GRBS, AND SHORT-GRB CONFUSION

A long GRB may be confused as a short GRB if only its brightest spikes with duration shorter than 2 s are above the background. To quantify such a tip-of-iceberg effect, we define an “effective amplitude” of a *long* GRB as

$$f_{\text{eff}} \equiv \frac{F'_p}{F_B}. \quad (2)$$

Here F'_p is the 1-second peak flux of a pseudo GRB, which is re-scaled down for multiplying by a factor ϵ ($\epsilon < 1$) from an original GRB lightcurve until its signal above the background has a duration $T_{90,\text{eff}}$ just shorter than 2 s. The physical meaning of the pseudo GRB is an otherwise identical GRB at the same redshift, except that the amplitude is lower by a factor ϵ . Since a short GRB has T_{90} shorter than 2 s, if one defines a f_{eff} parameter for a short GRB, it is identical to f . So we only define f_{eff} for long GRBs.

Technically, the f_{eff} parameter of a long GRB is measured based on the following procedure. 1. We extract the lightcurve of an observed GRB following the standard procedure with a time bin 64 ms; 2. We “re-scale” down the observed lightcurve to reduce the flux at each time bin by multiplying the flux by a factor ϵ ($\epsilon < 1$) for each time bin, and make a “signal” of a pseudo-GRB. 3. We simulate a Poisson background based on the extracted background information (the mean flux and standard deviation), and add this background to the “signal” and derive an “observed” lightcurve of the pseudo GRB; 4. For this simulated “observed” lightcurve, we apply the standard “curve of growth” method by accumulating net fluence above the background (e.g. von Kienlin et al. 2014). The duration T_{90} of the pseudo-GRB is obtained through measuring the time interval between 5% and 95% fluence; 5. We progressively multiply by a factor ϵ_i ($\epsilon_i < 1$) with the original light curve, each time record T_{90} until the derived T_{90} of the pseudo GRB is below 2 s. Record the f value of this pseudo GRB and define it as f_{eff} .

Figure 5 shows the long GRB 050525A as an example. The original burst is shown in Fig.5a, which has an $f = 9.43$. Figure 5b shows a pseudo GRB after re-scaling it down by a factor of $\epsilon = 0.06$. The signal (thin black curve in Fig.5b) is below the background level F_B (the gray curve). The sum of the signal and background gives a new “observed” lightcurve (the orange curve) of the pseudo GRB, whose T_{90} is measured through the curve of growth method. Only the main peak is within the 5% – 95% window. The measured T_{90} is just shorter than 2 s. We then measure the f value of this pseudo burst, which is the effective amplitude of the original burst. For this example, one measures $f_{\text{eff}} = 1.53$.

Figure 3b gives the 1D distributions of f_{eff} , and the T_{90} – f_{eff} distribution of long GRBs together with the T_{90} – f distribution of short GRBs in our sample. The f_{eff} values of long GRBs are systematically smaller than the f values of short GRBs. The f_{eff} distribution histogram of long GRBs is also shown in Fig.4a, which has a mean value $\bar{f}_{\text{eff}} = 1.24$,

² This flux level is usually slightly higher than the “true” background level due to the source contamination. However, this is not a concern for our analysis, since we are investigating the tip-of-iceberg effect with respect to the background at the detection time.

and the steepest slope $a = 8.04 \pm 1.23$ as compared with f distributions of long and short (see inset of Fig.4a).

One immediate conclusion from Fig.3b and Fig 4a is that the distribution of f_{eff} of long GRBs is very different from the f distribution of short GRBs. Most short GRBs have larger f values than the f_{eff} values of long GRBs. This suggests that the majority of short GRBs are *not* tip-of-iceberg of long GRBs. Instead, they reflect the intrinsically short duration of the central engine. Nonetheless, at smaller f values for short GRBs, confusion would appear since some long GRBs may show up as “disguised” short GRBs due to the tip-of-iceberg effect. In Fig.4b, we present the cumulative probability distribution of f for short GRBs and f_{eff} for long GRBs. It is clearly shown that most long GRBs have small f_{eff} values, e.g. $\sim 95\%$ below 1.5. In contrast, only $\sim 30\%$ short GRBs have $f < 1.5$.

In order to quantify the chance probability of disguised short GRBs, we carry out a Monte Carlo simulation. Since the observed short GRBs may include both intrinsic and disguised short GRBs, we assume an f distribution $N(f) \propto f^{-\alpha}$ for the intrinsic short GRBs, with the slope α taken as a parameter to be constrained by the data. We then simulate 10^4 short GRBs whose f distribution follows this distribution. Next, we simulate a certain amount of disguised short GRBs whose f -distribution satisfies the f_{eff} distribution of long GRBs. The observed short GRBs should be a superposition of the intrinsic and disguised short GRBs. In order to calibrate the two population, we notice that there are 7 observed short GRBs that have $f < 1.5$, and one of them (GRB 090426) is a disguised short GRB (Levesque et al. 2010; Xin et al. 2011; Thöne et al. 2011) with $f = 1.48$. The chance probability for a disguised short GRB at $f \leq 1.5$ is therefore $P(f < 1.5) \sim 1/7 \sim 0.142$. With this calibration, we obtain the “observed” short GRB sample by superposing the simulated intrinsic and disguised short GRB samples. We require that f distribution of this “observed sample” satisfies the observed f distribution, whose slope is ~ 1.66 . We find that the α value of the simulated intrinsic short GRBs is only slightly shallower, with $\alpha \sim 1.61$. This is understandable, since essentially all the observed short GRBs at $f > 1.5$ are intrinsic ones, and they define the slope of the f -distribution of the intrinsic short GRB sample. After reaching consistency with the data, we track the fraction of intrinsic and disguised short GRBs in the total simulated sample to map the chance probability of disguised short GRB below any f value. This probability function reads

$$P(< f) \sim 0.78_{-0.4}^{+0.71} f^{-4.33 \pm 1.84} \quad (3)$$

Since the f and f_{eff} distribution indices have errors, the chance probability in Eq.(3) also have errors. The coefficient error and the index error are correlated. All the relations in any case allow $P(f < 1.5) = 0.142$ (see Fig.4c). One can see that the chance probability for contamination can reach 78% near $f = 1$. So for detected short GRBs with a small f value (say $f < 1.5$), one should be cautious to draw conclusion about the duration category of the GRB.

It is interesting to note that GRB 060614 (Gehrels et al. 2006), the peculiar long GRB without supernova association, has $f_{\text{eff}} = 1.75$. This means that its tip-of-iceberg still has a large f to be consistent with the short GRB f distribution. Indeed, by scaling it down, it looks like a short GRB with

extended emission (Zhang et al. 2007b). Our analysis again supports the Type I (compact star) origin of this GRB.

4 THE $F_{\text{EFF},z}$ PARAMETER AND “REST-FRAME SHORT” GRBS

Some long GRBs have a rest-frame duration $T_{90}/(1+z) < 2$ s. The three GRBs with the highest redshifts, i.e. GRB 080913 (Greiner et al. 2009), GRB 090423 (Tanvir et al. 2009; Salvaterra et al. 2009), and GRB 090429B (Cucchiara et al. 2011) are all of this type, but likely have a Type II (massive star) origin based on the multi-wavelength criteria (Zhang et al. 2009). It would be very interesting to investigate whether this is also due to the tip-of-iceberg effect.

In order to check such a possibility, we define a third parameter

$$f_{\text{eff},z} \equiv \frac{F'_{p,z}}{F_B}. \quad (4)$$

Here $F'_{p,z}$ is the 1-second peak flux of a pseudo GRB, which is generated by “moving” the original GRB to progressively higher redshifts until the rest-frame duration $T_{90}/(1+z)$ becomes shorter than 2 s. A GRB, when moved to a higher redshift, would usually have a shorter rest frame duration, although the observed duration may not shrink due to time dilation (Kocevski & Petrosian 2013). In principle, it would always reach the “rest-frame-short” phase before completely disappearing beneath the background. It would be interesting to investigate the critical redshift z_c above which a burst appears as rest-frame-short.

Technically, moving a GRB with known redshift to higher redshifts is not straightforward. One needs to reduce the time-resolved spectra of the GRB, derive the correct spectral parameters, and perform a proper k -correction to the spectrum in order to obtain the BAT-band light curve of the pseudo GRB.

To carry out such an exercise, for each GRB with redshift measurement, we first apply *Xspec* to conduct a time-dependent spectral analysis to the raw data. We dissect the lightcurve into multiple time bins, with the bin size self-adjusted to allow a signal-to-noise ratio $S/N > 5$, so that the spectral parameters can be constrained. A typical GRB spectrum, if the observational band is wide enough, can be described as the Band function (Band et al. 1993; Abdo et al. 2009; Zhang et al. 2011). In order to perform a proper k correction, ideally one should know the Band spectral parameters α , β and E_p . However, since the BAT band is narrow, for most GRBs the spectra can be only fit by a cutoff power law or a single power law (Sakamoto et al. 2008, 2011). We therefore apply the following procedure to estimate the Band spectral parameters: 1. If a burst was also detected by *Fermi* GBM or *Konus* Wind, we adopt the spectral parameters measured by those instruments. 2. For those bursts that were not detected by other instruments but can be fit with a cutoff power law, we adopt the derived α and E_p parameters, and assume a typical value $\beta = -2.3$. 3. For those GRBs that could only be fit with a single power law, we have to derive E_p using an empirical correlation between the BAT-band photon index Γ^{BAT} and E_p , as derived previously for Swift GRBs (Sakamoto et al. 2009; Zhang et al.

2007a,b; Virgili et al. 2012). The typical parameters $\alpha = -1$, $\beta = -2.3$ are adopted to perform the simulations.

We note that moving a GRB to a higher z is effectively observing the rest-frame spectra in a higher energy band given the same observed BAT band. The spectral parameters β and E_p are therefore essential. These parameters are unfortunately usually not available for *Swift* GRBs. So our pseudo GRBs should be considered only as simulated GRBs rather than the original GRBs being moved to higher redshifts. In any case, such a simulation can serve the purpose of investigating the tip-of-iceberg selection effect. A similar simulation was carried out by Kocevski & Petrosian (2011).

Given the spectral parameters α , β and E_p of a particular GRB with known redshift z , we use the following procedure to simulate the pseudo GRB. First, we calculate the time-dependent bolometric burst luminosity using

$$L(t) = 4\pi D_L^2(z)F(t)k, \quad (5)$$

where $F(t)$ is the BAT-band, time-dependent flux, $D_L(z)$ is the luminosity distance to the source at the redshift z , and the k -correction factor corrects the BAT-band (15–150 keV) flux to a wide band in the burst rest frame ($1 - 10^4$ keV in this analysis), i.e.

$$k = \frac{\int_{1/1+z}^{10^4/1+z} EN(E)dE}{\int_{15}^{150} EN(E)dE}. \quad (6)$$

Here $N(E)$ is the time-dependent Band photon spectrum. To calculate $D_L(z)$, the concordance cosmology parameters ($H_0 = 71$ km s $^{-1}$ Mpc $^{-1}$, $\Omega_M = 0.30$, and $\Omega_\Lambda = 0.70$) are adopted.

Next, we apply the spectral model to calculate the BAT-band flux for a pseudo GRB at redshift z' . We keep the bolometric luminosity as a constant, and derive the BAT band flux using

$$F'(t') = \frac{L(t)}{4\pi D_L^2(z')k'}, \quad (7)$$

where

$$t' = \frac{1+z'}{1+z}t, \quad (8)$$

$D_L(z')$ is the luminosity distance to the source at redshift z' , and

$$k' = \frac{\int_{1/1+z'}^{10^4/1+z'} E'N(E')dE'}{\int_{15}^{150} E'N(E')dE'}. \quad (9)$$

Here $N(E')$ is the observed photon number spectrum of the pseudo GRB. The spectrum is still a Band function with the same α and β values. The only difference is that the peak energy is now shifted to $E'_p = E_p(1+z)/(1+z')$. We then add the background F_B and its fluctuation based on simulation, and re-calculate T_{90} of the pseudo GRB for each z' following the same procedure to derive f_{eff} . We then calculate the rest-frame duration using $T_{90}/(1+z)$.

By progressively increasing z' , we identify a critical redshift z_c beyond which $T_{90}/(1+z) < 2$ s is satisfied. The peak flux of the pseudo GRB at z_c is used to define $f_{\text{eff},z}$. We continue to increase the redshift, until the entire GRB disappears below the background. We record this redshift as z_{max} . The redshift range (z_c, z_{max}) is then where a rest-frame short GRB is observed.

The parameter $f_{\text{eff},z}$ depends on several parameters, such as $F(t)$ (which further depends on spectral parameters α , E_p , β or Γ^{BAT}), and F_B . We have introduced the error of each measurable, and properly derive the error of $f_{\text{eff},z}$ through error propagation.

As an example, we take the “naked-eye” GRB 080319B (Racusin et al. 2008) as the original burst and perform the simulation. The results are shown in Fig.6. The time-integrated γ -ray spectrum is well fit using a Band function, with $E_p = 675 \pm 22$ keV. The time-resolved of spectra are well obtained, with E_p evolving from ~ 740 keV to ~ 540 keV. The rest-frame isotropic energy release is $E_{\text{iso}} = (1.14 \pm 0.09) \times 10^{54}$ erg in the source frame $1 - 10^4$ keV band (Racusin et al. 2008, Amati et al. 2008).

We apply the above method to simulate pseudo GRBs with increasing redshifts. The lightcurves of the pseudo GRBs are presented in Fig.6a. Different colors denote different redshifts. From top to bottom, the redshifts are: $z = 0.937$ (original), 1, 2.3, 2.8, 3.6, 4.5, 5.1, and the critical redshift is $z_c = 5.53$. As shown in Fig.6a, the peak flux of the pseudo GRBs become progressively lower as z increases, and the observed durations initially become longer (due to time dilation) but later shrink (due to tip-of-iceberg effect). The rest-frame duration $T_{90}/(1+z)$ is found to decrease with redshift, similar to track with a smooth broken power-law (Fig.6b). At $z = z_c = 5.53$, $T_{90}/(1+z)$ becomes shorter than 2 s. We derive $f_{\text{eff},z} = 1.41$. The burst is no longer detectable at $z = z_{\text{max}} = 5.92$.

We carry out the same exercise for all the *Swift* GRBs with known redshifts. The $T_{90}/(1+z) - f_{\text{eff},z}$ diagram is presented in Fig.3c. We can see that $f_{\text{eff},z}$ are all below ~ 1.7 . It is interesting to note that the three highest- z GRBs (080913, 090423 and 090429B) and other rest-frame-short GRBs all have f values within this range. This suggests that they are simply the tip-of-iceberg of long GRBs. This conclusion is consistent with their Type II origin as derived from multi-wavelength arguments (Zhang et al. 2009). In Fig.7, we plot the histograms of z_c and z_{max} of all the GRBs in our analysis, and compare them with the z distribution of the detected rest-frame short GRBs. It is found that they are generally consistent with each other. The discrepancy in the high- z end (the distribution does not fully include the highest z GRB) may be due to the uncertainty of the high-energy spectra used in our simulations.

If the rest-frame short GRBs are the tip-of-iceberg of long GRBs, then the extended emission episodes (“icebergs” themselves) may show up in the softer X-ray band. To test this possibility, in Fig.8 we simulate the expected XRT band lightcurve of a pseudo naked-eye GRB 080319B at $z = z_c = 5.53$ (black). The same k -correction method has been applied. This is compared against the XRT-band lightcurves of the three highest- z GRBs (green for GRB 080913, blue for GRB 090423, and red for GRB 090429B), as well as the original XRT-band data of GRB 080319B (gray). It is seen that the XRT lightcurve of the pseudo GRB has an extended flaring episode extending to ~ 200 s followed by a steep decay, which is similar to the case of GRB 090423.

5 CONCLUSIONS AND DISCUSSION

In this paper, we propose to add “amplitude” as the third dimension as a complementary criterion to study GRB classification using the prompt emission data. We introduced three parameters, f (Eq.(1)), f_{eff} (Eq.(2)), and $f_{\text{eff},z}$ (Eq.(4)), to describe the amplitude of the original GRB and some simulated pseudo GRBs. We find the following interesting results:

- The f parameters for both long and short GRBs are distributed between 1 and about 10 as a rough power law. The paucity of low- f short GRBs may be understood as a trigger selection effect.
- The f parameter of many short GRBs is larger than the f_{eff} parameter of long GRBs. This suggests that most short GRBs are likely intrinsically short, and *not* simply the tip-of-iceberg of long GRBs.
- There is a confusion regime as f is small (e.g. < 1.5) for short GRBs, since intrinsically long GRBs may show up as disguised short GRBs due to the tip-of-iceberg effect. GRB 090426 is such an example. Through simulations, we derive the chance probability of disguised short GRBs as a function of f for short GRBs below a certain f value (Eq.[3]). The contamination becomes significant below $f \sim 1.5$, and can reach as large as $\sim 78\%$ at $f \sim 1$. This raises caution to judge the duration category of a short GRB with $f < 1.5$.
- When long GRBs are moved to high redshifts, they are likely observed as rest-frame short GRBs due to the “tip-of-iceberg” effect. These rest-frame short GRBs are supposed to have a low amplitude $f < 1.7$. The observed three highest- z GRBs and other rest-frame short GRBs all have such a low amplitude. So they are consistent with being tip-of-iceberg of long GRBs.

6 ACKNOWLEDGEMENTS

We thank the anonymous referee for helpful comments, and acknowledge the use of the public data from the *Swift* data archive. This work was supported by NASA NNX10AD48G, NNX14AF85G, and NSF AST-0908362 (BZ). EWL acknowledges support from the National Natural Science Foundation of China under grants No. 11063001, 10873002 and 11025313, the National Basic Research Program (“973” Program) of China (Grant 2009CB824800), Special Foundation for Distinguished Expert Program of Guangxi, the Guangxi SHI-BAI-QIAN project (Grant 2007201). BBZ acknowledges support by NASA SAO G01-12102X.

REFERENCES

Abdo A. A., et al., 2009, *Sci*, 323, 1688
 Amati L., et al., 2008, *MNRAS*, 391, 577
 Band D., et al., 1993, *ApJ*, 413, 281
 Barthelmy S. D., et al., 2005, *Natur*, 438, 994
 Berger, E. 2014, *ARAA*, in press (arXiv:)
 Berger E., et al., 2005, *ApJ*, 634, 501
 Bloom J. S., et al., 2006, *ApJ*, 638, 354
 Bonnell J. T., Norris J. P., Nemiroff R. J., Scargle J. D., 1997, *ApJ*, 490, 79
 Bromberg O., Nakar E., Piran T., Sari R., 2013, *ApJ*, 764, 179
 Campana S., et al., 2006, *Natur*, 442, 1008
 Cucchiara A., et al., 2011, *ApJ*, 736, 7

Cui X.-H., Nagataki S., Aoi J., Xu R.-X., 2012, *RAA*, 12, 1255
 Della Valle M., et al., 2006, *Natur*, 444, 1050
 Eichler D., Livio M., Piran T., Schramm D. N., 1989, *Natur*, 340, 126
 Fong W., Berger E., Fox D. B., 2010, *ApJ*, 708, 9
 Fox D. B., et al., 2005, *Natur*, 437, 845
 Fruchter A. S., et al., 2006, *Natur*, 441, 463
 Fynbo J. P. U., et al., 2006, *Natur*, 444, 1047
 Gal-Yam A., et al., 2006, *Natur*, 444, 1053
 Gehrels N., et al., 2004, *ApJ*, 611, 1005
 Gehrels N., et al., 2006, *Natur*, 444, 1044
 Gehrels N., et al., 2005, *Natur*, 437, 851
 Greiner J., et al., 2009, *ApJ*, 693, 1610
 Hakkila J., et al., 2000, *ApJ*, 538, 165
 Hjorth J., et al., 2003, *Natur*, 423, 847
 Horváth I., 1998, *ApJ*, 508, 757
 Horváth I., et al., 2010, *ApJ*, 713, 552
 Kann D. A., et al., 2011, *ApJ*, 734, 96
 Kocevski D., Petrosian V., 2013, *ApJ*, 765, 116
 Koshut T. M., et al., 1996, *ApJ*, 463, 570
 Kouveliotou C., et al., 1993, *ApJ*, 413, L101
 Lü H.-J., Liang E.-W., Zhang B.-B., Zhang B., 2010, *ApJ*, 725, 1965
 Levesque E. M., et al., 2010, *MNRAS*, 401, 963
 MacFadyen A. I., Woosley S. E., 1999, *ApJ*, 524, 262
 Mukherjee S., et al., 1998, *ApJ*, 508, 314
 Paczynski B., 1986, *ApJ*, 308, L43
 Paczynski B., 1991, *AcA*, 41, 157
 Paczynski B., 1991, *AcA*, 41, 257
 Pian E., et al., 2006, *Natur*, 442, 1011
 Qin Y., et al., 2013, *ApJ*, 763, 15
 Racusin J. L., et al., 2008, *Natur*, 455, 183
 Sakamoto T., et al., 2008, *ApJS*, 175, 179
 Sakamoto T., et al., 2011, *ApJS*, 195, 2
 Sakamoto T., et al., 2007, *ApJ*, 669, 1115
 Sakamoto T., et al., 2009, *ApJ*, 693, 922
 Salvaterra R., et al., 2009, *Natur*, 461, 1258
 Schmidt M., 2001, *ApJ*, 552, 36
 Schmidt M., Higdon J. C., Hueter G., 1988, *ApJ*, 329, L85
 Stanek K. Z., et al., 2003, *ApJ*, 591, L17
 Tanvir N. R., et al., 2009, *Natur*, 461, 1254
 Thöne C. C., et al., 2011, *MNRAS*, 414, 479
 Virgili F. J., Qin Y., Zhang B., Liang E., 2012, *MNRAS*, 424, 2821
 Woosley S. E., 1993, *ApJ*, 405, 273
 Xin L.-P., et al., 2011, *MNRAS*, 410, 27
 Xu, D. et al. 2013, *ApJ*, in press (arXiv:1305.6832)
 Zhang B.-B., et al., 2011, *ApJ*, 730, 141
 Zhang B., 2012, *IAUS*, 279, 102
 Zhang B., 2006, *Natur*, 444, 1010
 Zhang B., et al., 2007, *ApJ*, 655, 989
 Zhang B., et al., 2007, *ApJ*, 655, L25
 Zhang B., et al., 2009, *ApJ*, 703, 1696
 Zhang F.-W., Shao L., Yan J.-Z., Wei D.-M., 2012, *ApJ*, 750, 88

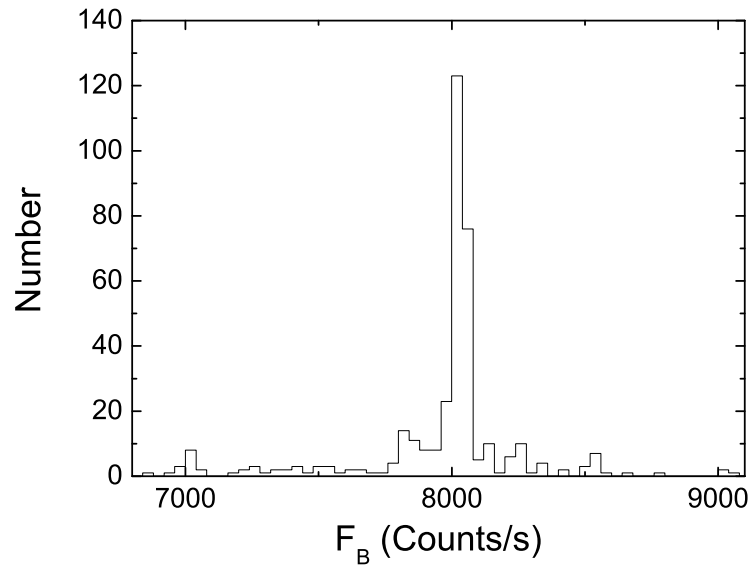


Figure 1. The the histogram of F_B for all the GRBs in our sample.

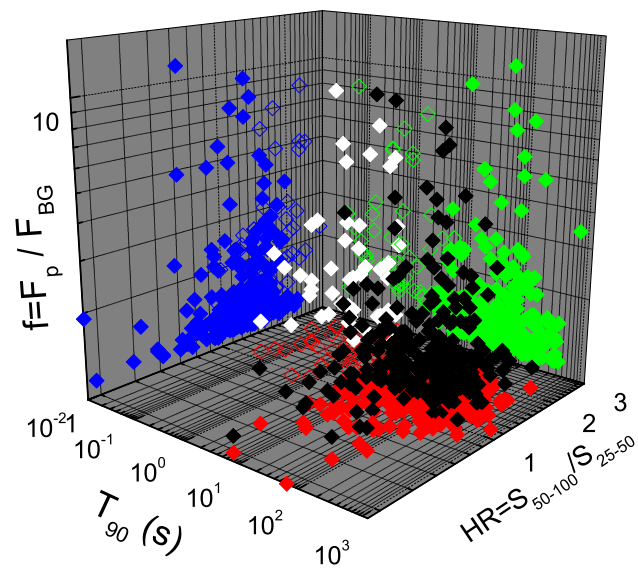


Figure 2. The $T_{90} - HR - f$ 3D distribution of the *Swift* GRBs in our sample. Long and short GRBs are denoted as solid black and white diamonds, respectively. Their projections to the $T_{90} - HR$, $T_{90} - f$, and $HR - f$ 2D planes are denoted in red, green and blue colors, respectively, with the long and short GRBs denoted with solid and open symbols, respectively.

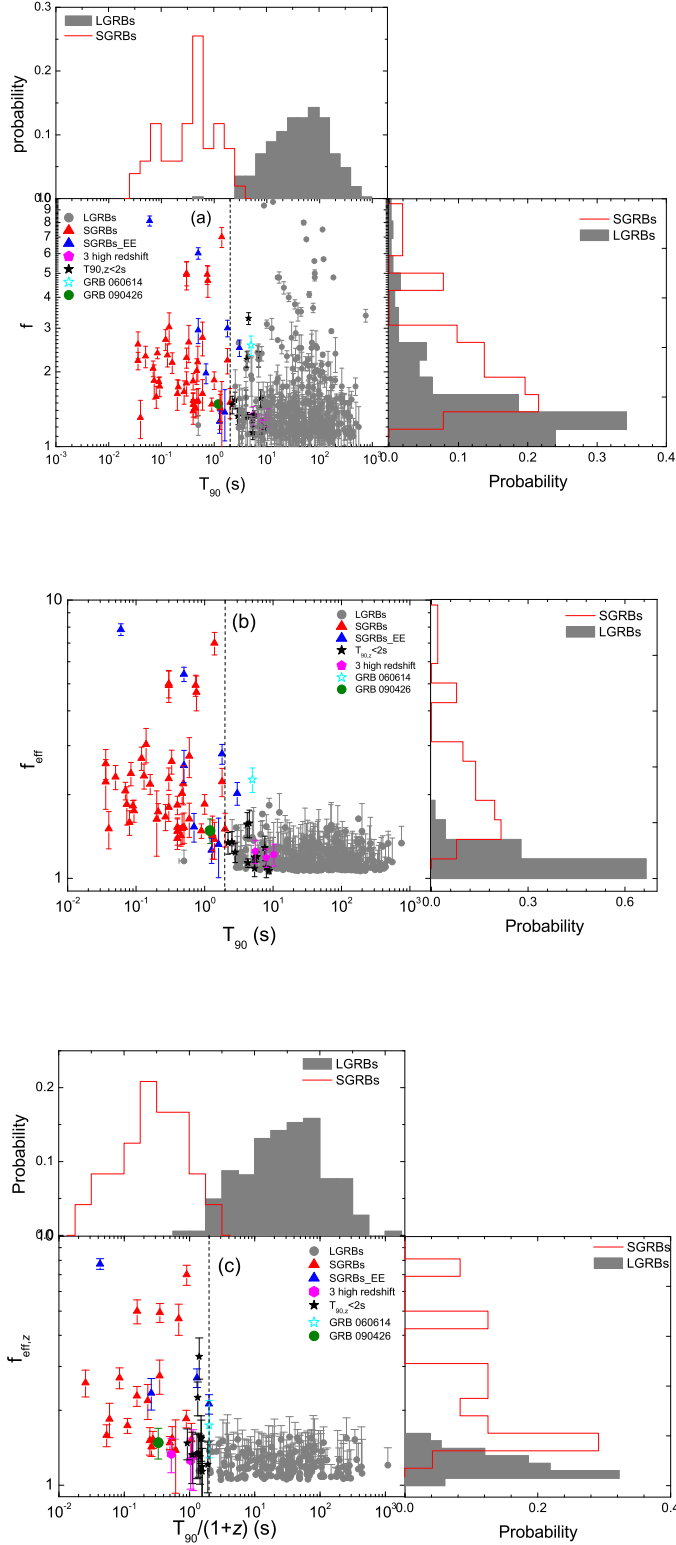


Figure 3. The 1D and 2D distributions for the bursts in our sample. (a): The $T_{90} - f$ diagram of the GRBs in our sample. (b) The $T_{90} - f_{\text{eff}}$ diagram of GRBs in our sample. (c) The $T_{90}/(1+z) - f_{\text{eff},z}$ diagram of GRBs in our sample. The following convention is adopted for all three plots: Gray: long GRBs, red: short GRBs; blue: short GRBs with extended emission; purple: three GRBs with the highest z ; black: “rest-frame short” GRBs. GRB 060614 and GRB 090426 are marked with special symbols. The vertical dashed line is the 2 s separation line.

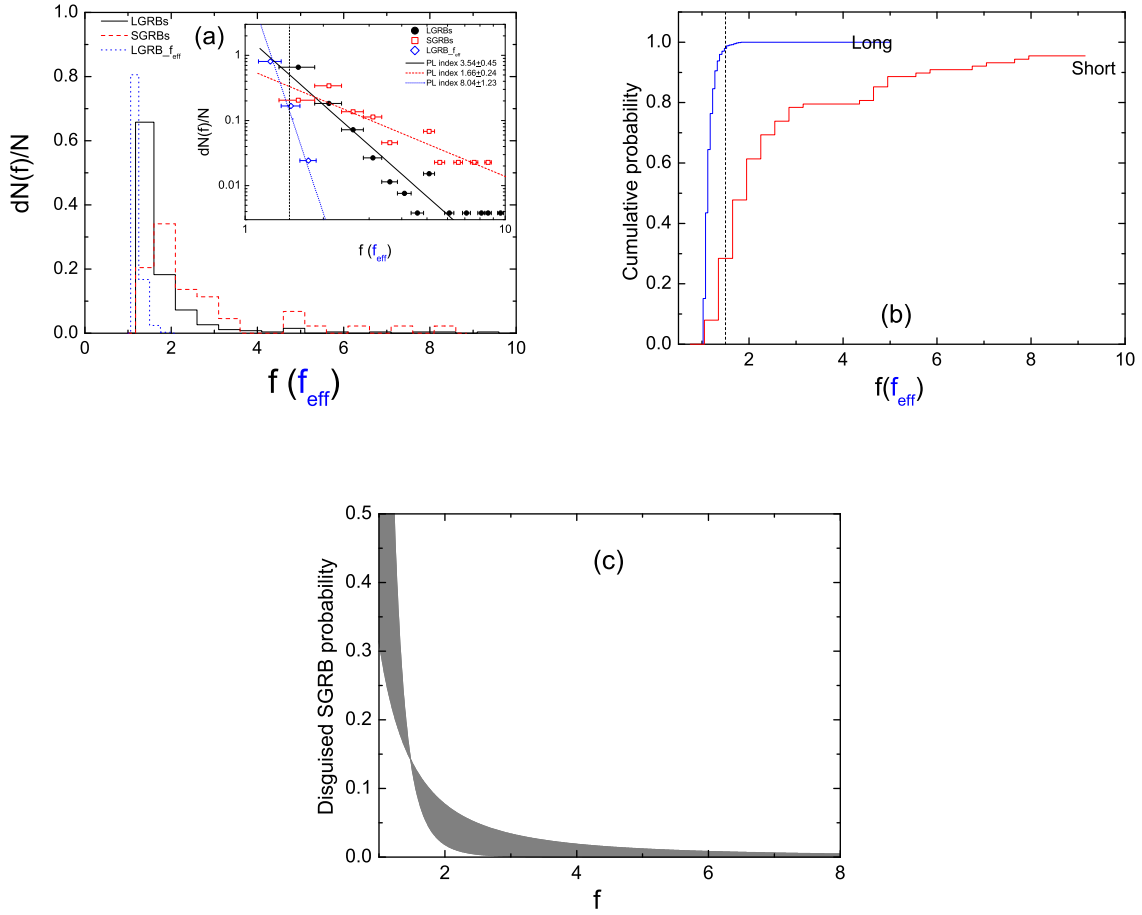


Figure 4. (a) The distributions of f (for both long and short GRBs) and f_{eff} (for long GRBs only) as well as their power law fits (inset). (b) The cumulative probability of a GRB below a certain f (for short GRBs) or f_{eff} (for long GRBs) value. The vertical line corresponds to $f = 1.5$. (c) Chance probability of a disguised short GRB below a certain f value. The gray region is the error zone for the probability.

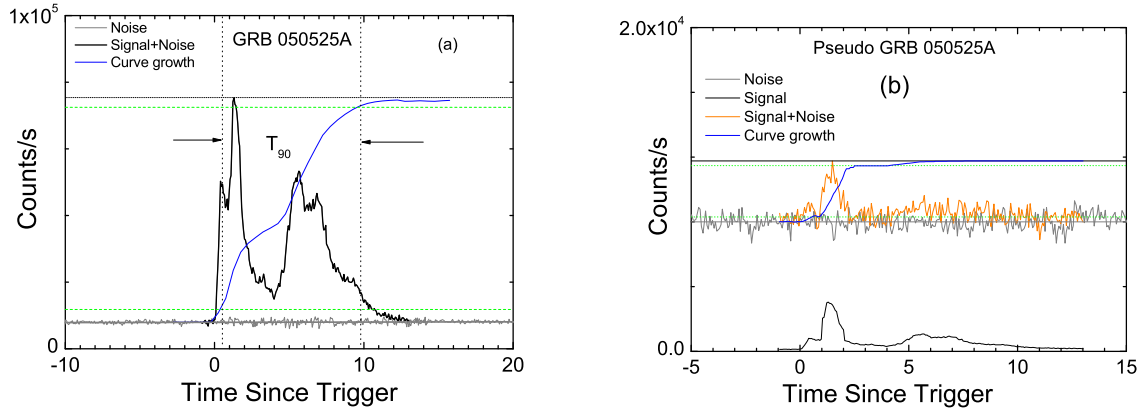


Figure 5. An example of defining f_{eff} with GRB 050525A. (a) The original lightcurve and the definition of T_{90} using the standard “curve of growth” method. (b) The pseudo GRB generated from GRB 050525A. The original lightcurve is scaled-down by a factor of 0.06 (thin black curve). Adding the background (grey), the total lightcurve (orange curve) is the “observed” lightcurve of the pseudo GRB. Applying the curve of growth method, the T_{90} of the pseudo GRB is just shorter than 2 s. The f parameter of the pseudo GRB, which is f_{eff} of GRB 050525A, is measure as 1.53.

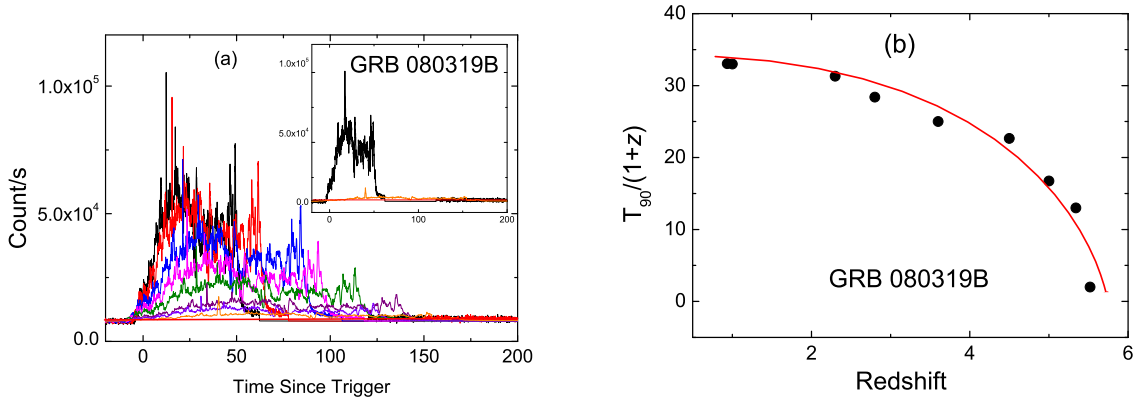


Figure 6. (a) The simulated BAT-band pseudo GRB lightcurves by moving GRB 080319B to progressively high redshifts. From top to bottom, $z = 0.937, 1, 2.3, 2.8, 3.6, 4.5, 5.1, 5.53$. (b) The measured rest-frame duration $T_{90}/(1+z)$ of the pseudo GRBs in our simulation. The red solid line shows a smooth broken power-law fit.

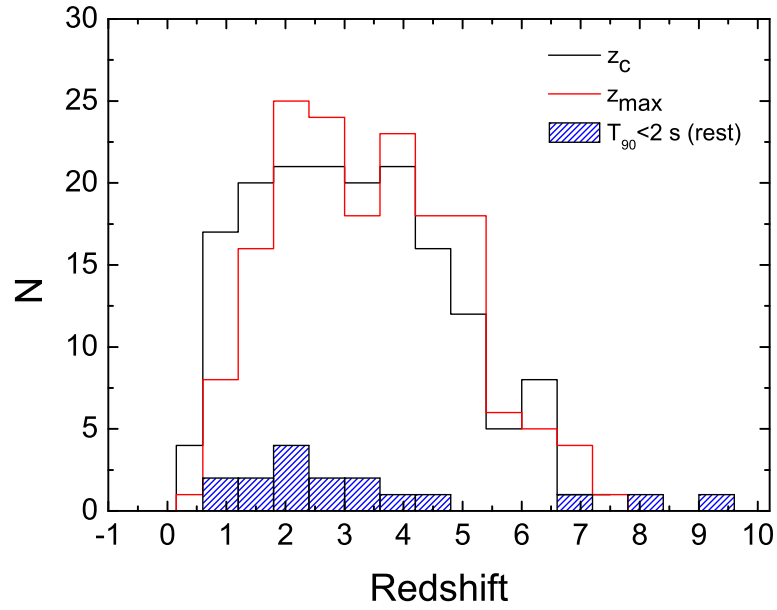


Figure 7. The distributions of z_c and z_{\max} for the simulated pseudo GRBs as compared with the redshift distribution of the observed rest-frame short GRBs.

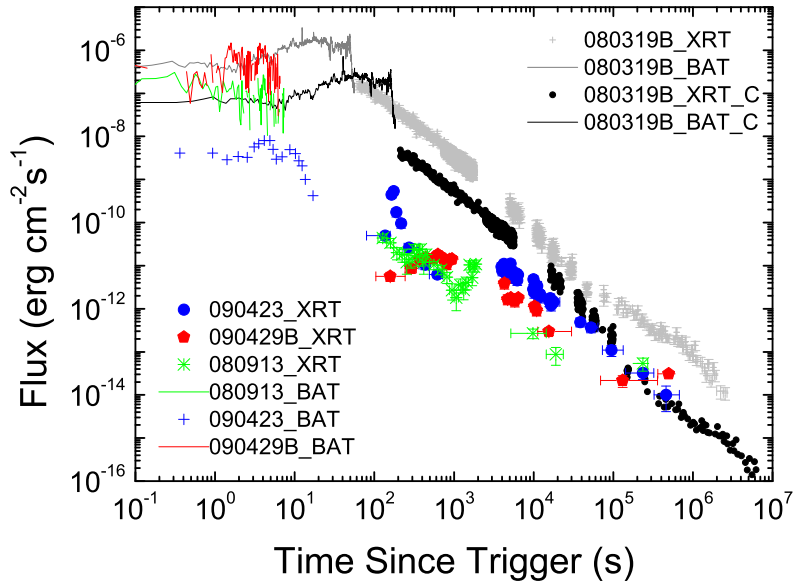


Figure 8. The simulated XRT-band lightcurve of the pseudo GRB by moving GRB 080319B to $z = z_c = 5.53$ (black), as compared with the original XRT-band lightcurves of GRB 080319B (gray), GRB 080913 (green), GRB 090423 (blue), and GRB 090429B (red).